# Supplementary Information for "Anomalous enhancement of charge density wave in kagome superconductor $CsV_3Sb_5$ approaching the 2D limit"


Boqin Song[1,*], Tianping Ying[2,*✉], Xianxin Wu[3,*], Wei Xia[4,5,*], Qiangwei Yin[6,*], Qinghua Zhang[2], Yanpeng Song[2], Xiaofan Yang[1], Jiangang Guo[2], Lin Gu[2], Xiaolong Chen[2], Jiangping Hu[2], Andreas P. Schnyder[7], Hechang Lei[6✉], Yanfeng Guo[4✉], and Shiyan Li[1,8,9✉]

[1]*State Key Laboratory of Surface Physics, Department of Physics, Fudan University, Shanghai 200433, China*

[2]*Beijing National Laboratory for Condensed Matter Physics, Institute of Physics, Chinese Academy of Sciences, Beijing 100190, China*

[3]*CAS Key Laboratory of Theoretical Physics, Institute of Theoretical Physics, Chinese Academy of Sciences, Beijing 100190, China*

[4]*School of Physical Science and Technology, ShanghaiTech University, Shanghai 201210, China*

[5]*ShanghaiTech Laboratory for Topological Physics, Shanghai 201210, China*

[6]*Laboratory for Neutron Scattering, and Beijing Key Laboratory of Optoelectronic Functional Materials MicroNano Devices, Department of Physics, Renmin University of China, Beijing 100872, China*

[7]*Max-Planck-Institut für Festkörperforschung, Heisenbergstrasse 1, D-70569 Stuttgart, Germany*

[8]*Collaborative Innovation Center of Advanced Microstructures, Nanjing 210093, China.*

[9]*Shanghai Research Center for Quantum Sciences, Shanghai 201315, China*

## Supplementary Note 1: **TEM image of the transverse section of $CsV_3Sb_5$ thin flakes**

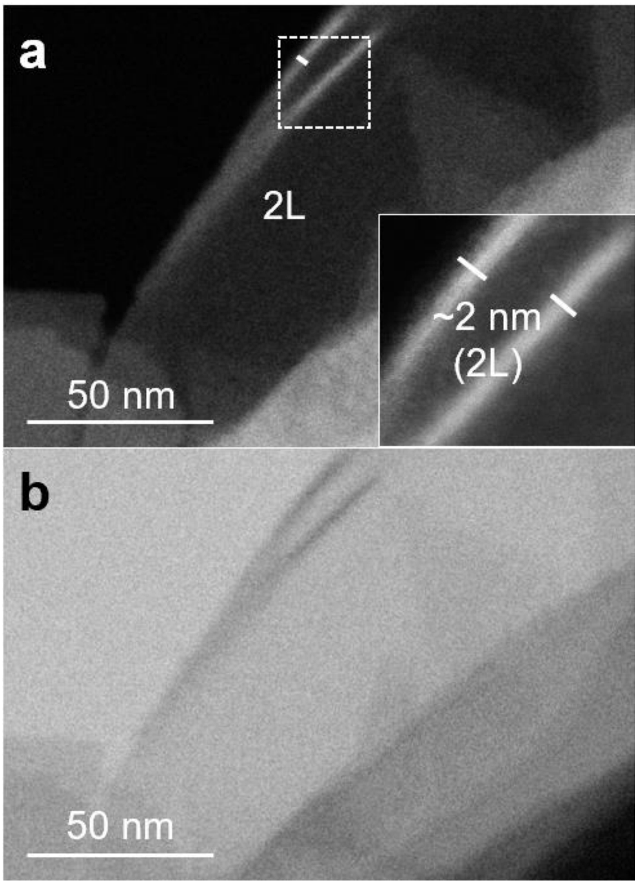


**Supplementary Figure 1 | Transverse section of $CsV_3Sb_5$ atomic thin flakes. a, b** Low-magnification ADF (**a**) and ABF (**b**) STEM images of the edge of the exfoliated $CsV_3Sb_5$ thin flake. The short white lines are the transverse section of the curled edge part.

To answer the question of whether the $V_3Sb_5$ kagome layer can survive when approaching the atomic limit, we employ the STEM to check the crystallinity in the atomic-thin flakes. We find the edge area will naturally curl to expose its transverse section. Supplementary Fig. 1 shows the morphology of the edge area. It is determined to be a 2L flake from the length (white lines) considering the lattice parameter $c = 9.8$ Å. Thus, we can use its intensity contrast as a gauge to determine the thickness of other thin flakes.

## Supplementary Note 2: Thickness determination in TEM

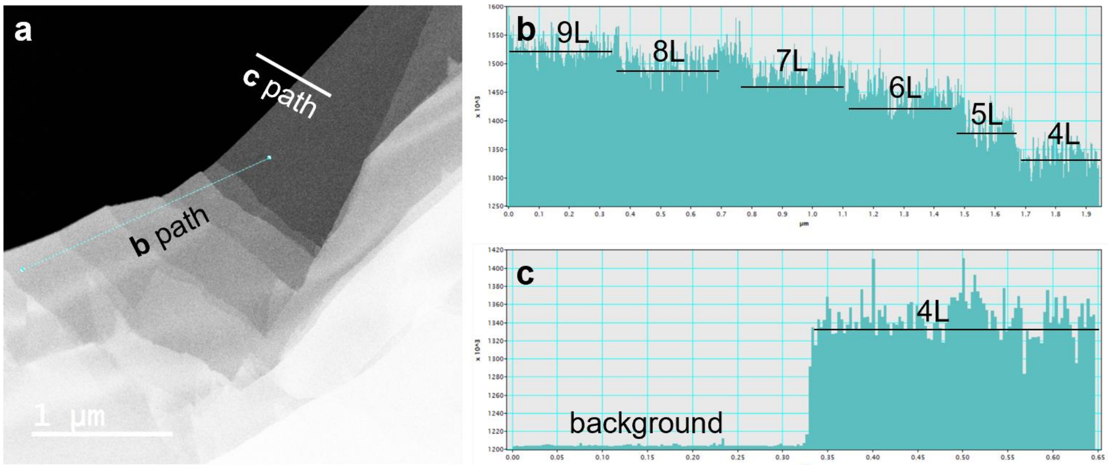


**Supplementary Figure 2 | Determination of the flake thickness. a** Low-Magnification STEM image of the exfoliated flakes. **b, c** Line profile of ADF intensity along different paths shown in **a**.

Supplementary Fig. 2a illustrates the low magnification STEM image of an exfoliated sample with a stair structure. With the intensity contrast gauge obtained in Supplementary Note 1, we can determine the thickness of each step of the stair from the ADF intensity line profile plotted in Supplementary Fig. 2b, c. A few flat areas with certain thicknesses can be selected for SAED and ABF-STEM measurements (see main text Fig. 1c, d).

## Supplementary Note 3: Quantitative analysis of the exfoliated thin flakes

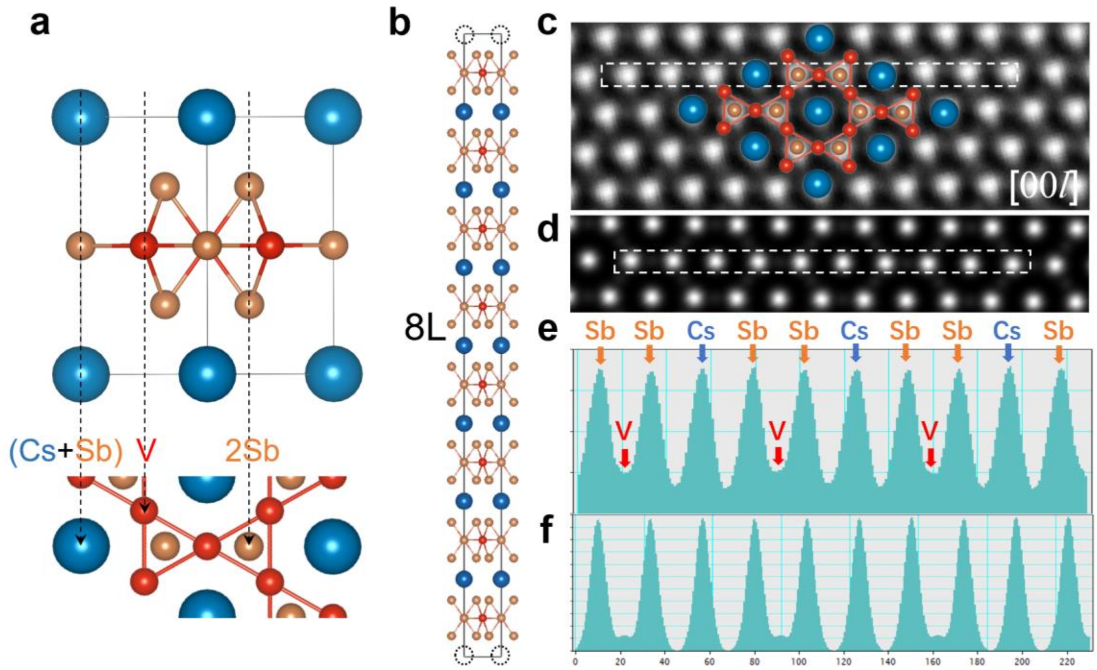


**Supplementary Figure 3 | Quantitative analysis of the 8L sample. a** Side view of the $CsV_3Sb_5$ structure along the [110] direction. Dotted arrows indicate the direction of the projection along the *c* axis. **b** Schematical structure of an 8L sample. Open circles on the out-most of the sample illustrate the loss of surface Cs. **c, d** HAADF-STEM image along the *c* axis. The crystal structure is superimposed. **e, f** Intensity line profile of the region marked by the dotted line shown in **c** and **d**.

STM studies found a fully occupied Cs surface layer can be unstable, often leading to randomly distributed Cs atoms that prone to clustering[1]. Loss of surface Cs distinctly manipulate the VHS relative to the Fermi surface, especially in the thin flakes[2]. On the other hand, Cs layers bond the $V_3Sb_5$ layers together, preventing interlayer slide. Therefore, it is interesting to investigate the stability of Cs layers between the $V_3Sb_5$ kagome layers in these free-standing thin flakes. Supplementary Fig. 3c, d show the HAADF-STEM image of an 8L flake along the *c* axis. The clear atomic resolution image negates the possibility of interlayer slide. Hence, we can use the primary crystal structure to calculate the number of the elements, as shown in Supplementary Fig. 3a. Intensity lines of the marked region are plotted in Supplementary Fig. 3e, f. The integrated intensity is proportional to $Z^2$, where Z is the atomic number of the elements. Comparing the intensity with atomic number, a model of 8L sample without the outmost Cs layers corresponds best, as shown in Supplementary Fig. 3b.

## Supplementary Note 4: Devices fabrication

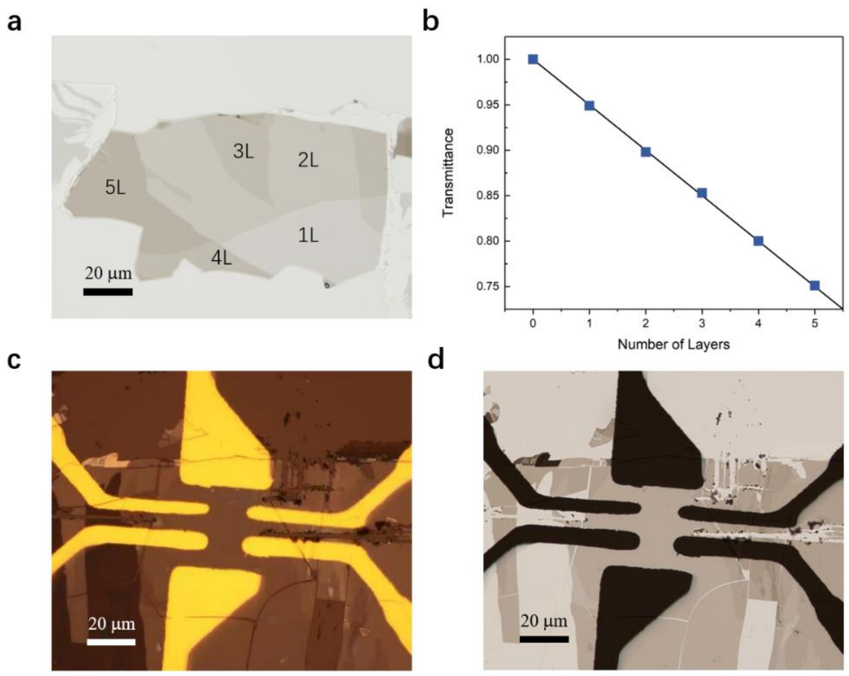


**Supplementary Figure 4 | $CsV_3Sb_5$ thin-flake device fabrication. a** Optical image of few-layer flakes of $CsV_3Sb_5$ cleaved onto thermally evaporated $Al_2O_3$ thin film (thickness ~70 nm). The $CsV_3Sb_5/Al_2O_3$ stack is supported on a sapphire substrate. Image was taken in transmission mode. Number of layers is labeled on the selected areas with the scale bar of 20 μm. **b** Transmittance as a function of the number of layers. The transmittance (filled squares) follows the Beer-Lambert law (solid line). **c**, **d** Optical image of a device in reflection and transmission mode, respectively. Metal (Cr/Au) contacts to the sample were thermally evaporated through a stencil mask. Excess $CsV_3Sb_5$ flake that shorts adjacent electrodes are removed with a sharp tip.

We obtain few-layer $CsV_3Sb_5$ samples using an $Al_2O_3$-assisted exfoliation technique[3]. Firstly, an $Al_2O_3$ thin film is thermally evaporated onto a freshly prepared surface of the bulk crystal. Then, we lift the $Al_2O_3$ thin film using a thermal release tape, accompanied by $CsV_3Sb_5$ thin flakes cleaved from the bulk crystal. Subsequently, the $Al_2O_3/CsV_3Sb_5$ stack is released onto a piece of polydimethylsiloxane (PDMS) with the $CsV_3Sb_5$ side in contact with the PDMS surface. The thin flakes are finally stamped assembly onto a sapphire substrate and inspected under an optical microscope in transmission mode. Supplementary Fig. 4a displays an typical optical image of few-layer $CsV_3Sb_5$ flakes on $Al_2O_3$ film on a sapphire substrate. We determined the layer number of the flakes with an atomic force microscope (AFM) and optical contrast. Here the optical contrast is transmittance defined as $G^{\mathrm{T}}_{\mathrm{sample}}/G^{\mathrm{T}}_{\mathrm{substrate}}$, where $G^{\mathrm{T}}_{\mathrm{sample}}$ and $G^{\mathrm{T}}_{\mathrm{substrate}}$ are the intensity of the transmission (T) through the sample and substrate, respectively, in blue channel of the image captured with a charge-coupled device (CCD) camera. The transmittance of various numbers of layers follows the Beer-Lambert Law (Supplementary Fig. 4b), which enables us to determine the layer number quickly and precisely. After that, we deposit Cr/Au contacts through a stencil mask on the thin flakes for transport measurements (Supplementary Fig. 4c,d).

## Supplementary Note 5: Stability of the thin-flakes device

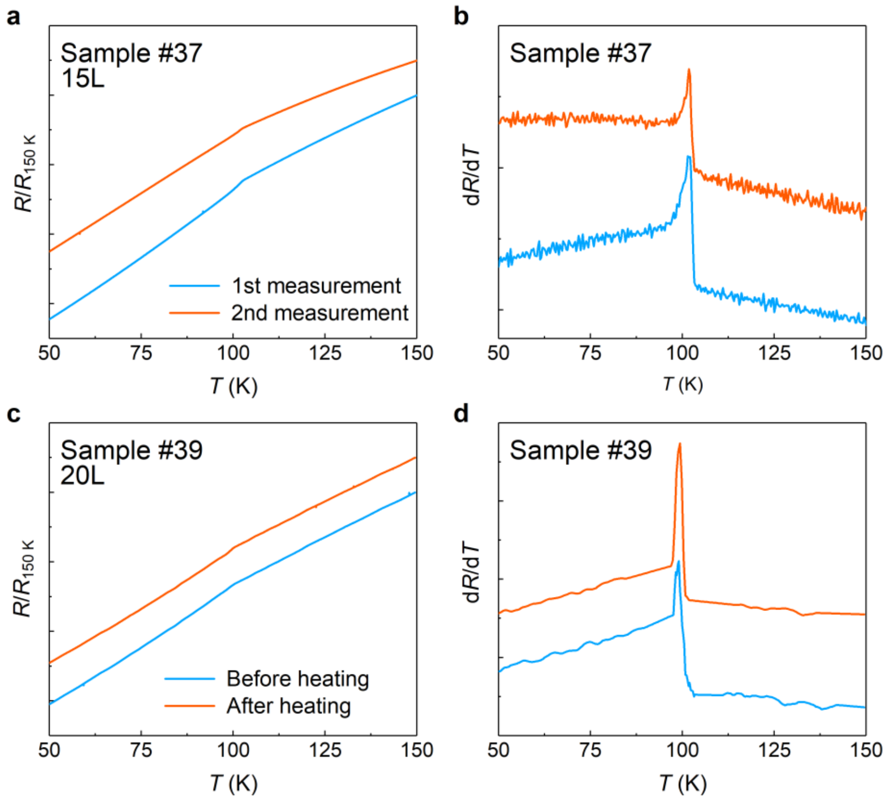


**Supplementary Figure 5 | Stability of the thin-flake devices. a** A 15L sample measured immediately after the nano fabrication (1st) and 40 days stored in a glove box (2nd). **c** A 20L sample measured before and after heating at 120 °C for half an hour in a high vacuum chamber. **b**, **d** Derivation of resistance in **a** and **c**. The highly reproducible kink temperature illustrates the stability of the fabricated devices. Lines in **a-d** are all shifted vertically for clarity.

To eliminate the influence of remnant oxygen in glove box and heating degradation (thermal release) towards sample quality during our fabrication process, we examined the stability of the devices. Supplementary Fig. 5a shows the normalized resistance of sample #37 just fabricated (blue line) and stored in a glove box for 40 days (orange line). Despite the slope becoming a little gentler below $T_{CDW}$, the peak of the derivative maintains its position (Supplementary Fig. 5b), indicating adequate stability for fabrication process (3 hours generally). Thermal stability is tested on sample #39. The slope of normalized resistance and the $T_{CDW}$ remains the same before and after heating at 120 °C (used in thermal release) in a high vacuum chamber (Supplementary Fig. 5c, d), revealing excellent stability of the fabricated thin-flake devices against thermal fluctuations.

## Supplementary Note 6: Hall measurement and anomalous Hall extraction

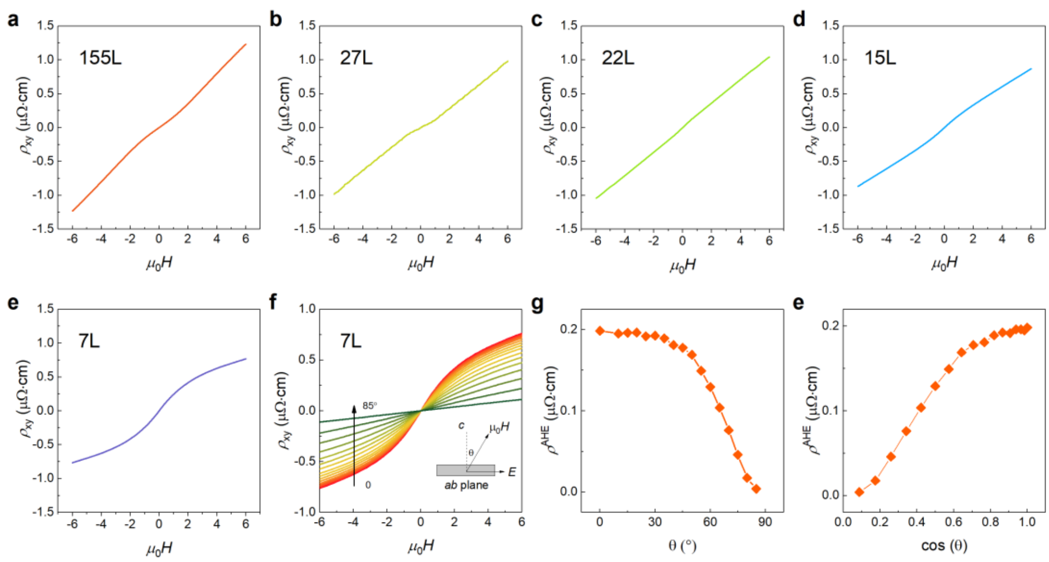


**Supplementary Figure 6 | Hall measurement of various $CsV_3Sb_5$ flakes. a-e** Raw Hall data of Fig. 2d in main text. **f** Hall resistivity as the variation of angle θ between magnetic field and *c* axis. The inset is a schematic configuration of magnetic field relative to the applied electrical field. All $\rho_{xy}$ in **a-f** are measured at 5 K. **g**, **e** Extracted Anomalous Hall resistivity against θ and the out-of-plane component of magnetic field (cos(θ)), respectively.

Supplementary Fig. 6a-e sketch Hall resistivity of $CsV_3Sb_5$ flakes with various thicknesses. It can be roughly seen that the anomalous Hall resistivity decreases to negligible and show a sign change with the reduction of sample thickness. However, the normal Hall at high-field does not change its sign. To clearly illustrate the anomalous Hall effect in $CsV_3Sb_5$ thin flakes, we extract the anomalous Hall term from the $\rho_{xy}$ by subtracting the local linear term and plot them in Fig. 2d of the main text. To further confirm the AHE nature of sign-changed data of thin flakes, we carry out an angle-dependent measurement in a 7L sample. Supplementary Fig. 6f shows the $\rho_{xy}$ varied with the angle θ between the magnetic field and the *c* axis. Supplementary Fig. 6g, e show the $\rho^{AHE}$ dependence on θ and cos(θ), respectively. The AHC is angle independent until magnetic field is tiled away from the *c* axis by about 30°, then it rapidly decreases to 0. $\rho^{AHE}$ cannot be scale linearly with the out-of-plane component of magnetic field (cos(θ)), confirming the AHE origin of the skewed Hall resistivity at low field in atomically thin flakes and the AHE extraction is correct.

## Supplementary Note 7: Coulomb gap in atomically thin flakes

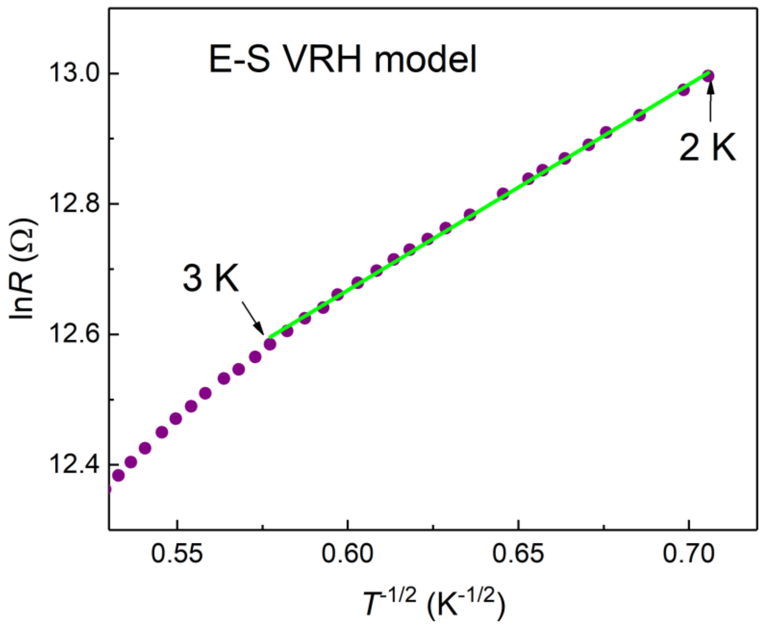


**Supplementary Figure 7 | E-S VRH model fitting of the 2L sample.** The resistance of the 2L sample below 3 K deviates from the 2D VRH model. But it can be fitted by the E-S VRH model which is a hallmark of the opening of a coulomb gap.

The non-metallic resistance in the 2L sample cannot be fitted by a band gap model, but follows a 2D variable-range-hopping behavior at the temperature range 4-40 K shown in Fig. 4a of the main text[4]. Supplementary Fig. 7 shows the fitting of the resistance below 3 K using the Efros-Shklovskii variable-range-hopping model[5]. The linear fit of the low-temperature region indicates the opening of a Coulomb gap induced by enhanced repulsive interaction. It can be understood as a direct consequence of dimension reduction with reduced carrier concentration, which eventually drives the MIT.

## Supplementary References


1. Zhao, H. et al. Cascade of correlated electron states in the Kagome superconductor $CsV_3Sb_5$. *Nature* **599**, 216–221 (2021).
2. Song, Y. et al. Competition of Superconductivity and Charge Density Wave in Selective Oxidized $CsV_3Sb_5$ Thin Flakes. *Phys. Rev. Lett.* **127**, 237001 (2021).
3. Deng, Y. et al. Gate-tunable room-temperature ferromagnetism in two-dimensional $Fe_3GeTe_2$. *Nature* **563**, 94–99 (2018).
4. Mott, N. F. Conduction in glasses containing transition metal ions. *J. Non-cryst. Solids* **1**, 1–17 (1968).
5. Efros, A. L. & Shklovskii, B. I. Coulomb gap and low temperature conductivity of disordered systems. *J. Phys. C: Solid State Phys.* **8**, L49 (1975).